CHAPTER 16

Coupled Electrohydraulic Analysis Using Systems Models

Airplanes, automobiles, tractors, ships, robots, and other vehicles commonly contain hydraulic actuation systems such as brakes. Besides such *mobile hydraulic* systems, hydraulics is also common in stationary applications such as factories and elevators. In many cases, especially with computer control, the input to the hydraulic system is electrical. Such coupled systems are called *electrohydraulic systems*. The usual coupling devices are magnetic actuators and sensors.

16.1 COMPARING HYDRAULICS AND MAGNETICS

Hydraulic actuation systems have certain advantages over magnetic actuators [1]. As discussed in Chapter 5, magnetic pressures on steel surfaces are given by:

$$P_{\text{mag}} = B^2/(2\mu_o) - w_{\text{co}} \tag{16.1}$$

where coenergy w_{co} appears as in (5.17) and (5.13). The magnetic pressure P_{mag} of a typical steel was graphed in Figure 5.7 and shown to be less than 20 bar, even for magnetic flux densities B as large as 2.4 T. Recall that one bar equals 1.E5 Pa, which approximates the standard atmospheric pressure at sea level.

In comparison, hydraulic pressures of hundreds of bar are commonly used. Since force is pressure times area, the higher hydraulic pressures can yield smaller, lighter, and less expensive actuators than magnetic actuators. High hydraulic pressures produce high forces.

Another big advantage of hydraulic actuators is that magnetic actuator armatures often must be made of steel, a heavy material that reduces acceleration. Since acceleration must be high for fast actuation, armatures made of lighter material such as aluminum are advantageous. Hydraulic armatures do not carry any magnetic flux and need not be made of steel, and thus for a given force can produce faster acceleration.

Pure hydraulic systems, however, have the disadvantage of requiring a mechanical input, as shown in Figure 16.1. A typical example of Figure 16.1 is the automobile

Magnetic Actuators and Sensors, Second Edition. John R. Brauer.

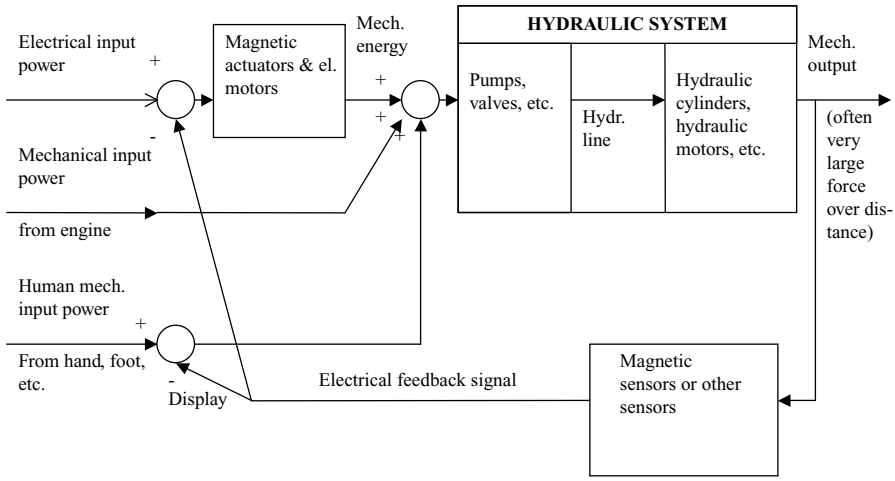

FIGURE 16.1 Block diagram showing energy conversions in a general system that includes a hydraulic system. The circles represent summing junctions. As shown, magnetic actuators require input electrical energy, which is not necessarily required by magnetic sensors with permanent magnets. The sensors may illuminate a display, such as vehicle speed, which is read by the human operator and thus used as one form of feedback control.

brake. The required large braking force can be produced by hydraulic cylinders, but in early days the only input was the human foot for the so-called manual brakes. Later, power brakes used the mechanical power of the gasoline engine to power a pump to provide additional hydraulic braking power. Nowadays, electric motors are often used to provide the power, and as discussed in Chapter 10, magnetic actuators and sensors are used for braking feedback control.

The most common way of utilizing electric power as well as optional computer control is through the magnetically operated hydraulic valve, which will be discussed later in this chapter. Thus coupled electrohydraulic systems are becoming more and more popular.

In converting energy from mechanical to hydraulic and back again, some energy is inevitably lost. Yet if the force output of Figure 16.1 is not large enough, a second hydraulic system can be added as a second hydraulic *stage*. While such multistage systems have been common in the past to produce large forces in large aircraft and tractors, to increase efficiency the trend nowadays is toward one stage that uses electrohydraulics.

16.2 HYDRAULIC BASICS AND ELECTRICAL ANALOGIES

As discussed in the preceding chapter, analogies are helpful in modeling various types of physical systems. Table 16.1 compares various physical system relationships, with its last column containing hydraulic relationships [2].

TABLE 16.1 Physical System Relationships

Parameter	Electrical	Mechanical (Linear)	Mechanical (Rotary)	Hydraulic
Inductance	L	M (mass)	J (inertia)	I (fluid inertia)
Units	henrys	kg	N m s^2	N s^2/m^5
Equation	$V = L\,di/dt$	$F = M\,dv/dt$	$T = J\,d\omega/dt$	$p = I\,dQ/dt$
Energy	$W = Li^2/2$	$W = Mv^2/2$	$W = J\omega^2/2$	$W = IQ^2/2$
Capacitance	C	K (spring)	K (spring)	C (capacitance)
Units	farads	N/m	N m/rad	m^3/Pa
Equation	$V = (1/C)\int i\,dt$	$F = Kx$	$T = K\theta$	$p = (1/C)\int q\,dt$
Energy	$W = CV^2/2$	$W = Kx^2/2$	$W = K\theta^2/2$	$W = Cp^2/2$
Resistance[a]	R	B (damper)	B (damper)	Orifice
Units	Ω (ohms)	N/m/s	N m s	$(m^3/s)/(N/m^2)^{1/2}$
Equation	$V = IR$	$F = Bv$	$T = B\omega$	$Q = Kvp^{1/2}$
Power	$P = V^2/R$	$P = Bv^2$	$P = B\omega^2$	$P = pQ$
Effort	V (voltage)	F (force)	T (torque)	p (pressure)
Units	V	N	N-m	Pa (= N/m^2)
Equation	$\int V\,dt = LI$	$\int F\,dt = mv$	$\int T\,dt = J\omega$	$\int p\,dt = QI$
Flow	I (current)	v (velocity)	ω (angular velocity)	Q (flow rate)
Units	amperes	m/s	rad/s	m^3/s
Equation	$\int I\,dt = q$	$\int v\,dt = x$	$\int \omega\,dt = \theta$	$\int Q\,dt = q$
Power	$P = VI$	$P = Fv$	$P = T\omega$	$P = pQ$

[a]Turbulent resistance.

Just as standard symbols are used worldwide for electric circuit elements such as resistors, inductors, and capacitors, hydraulic circuits have standard symbols. Like wires in electric circuits, hydraulics lines and hoses are represented by lines.

Figure 16.2 shows several common hydraulic ISO standard symbols. The tank shown in Figure 16.2 is generally at zero pressure, similar to ground in electric circuits. As indicated in Table 16.1, pressure P in hydraulic circuits is analogous to voltage, and fluid flow rate Q is analogous to current. The pressure source is usually a pump. Some types of pumps (such as in artificial hearts) require reciprocating motion and are thus operated by reciprocating magnetic actuators. More often, however,

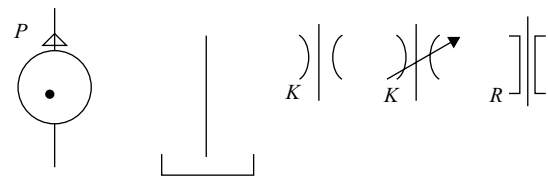

FIGURE 16.2 Symbols are shown above for several hydraulic components. From left to right they are: pressure source (e.g., a pressure-compensated pump), hydraulic line and tank, common orifice (turbulent flow with square law relation in Table 16.1), control valve (variable turbulent orifice), and linear (laminar) orifice.

pumps are powered by rotary machines such as internal combustion engines or electric motors.

Analogous to electrical capacitance is hydraulic capacitance, obtained by storage devices such as accumulators. While hydraulic capacitance is common, hydraulic inductance is usually negligible.

Analogous to the electrical resistor is the hydraulic orifice, a narrowing of a hydraulic line. For a linear orifice:

$$P = QR \tag{16.2}$$

The more common nonlinear orifice obeys the relation in Table 16.1:

$$P = (Q/K)^2 \tag{16.3}$$

The nonlinear orifice contains turbulent flow, while linear orifices contain laminar flow [3–5]. As shown in Figure 16.2, the two orifice types have differing symbols. Also shown in Figure 16.2, an orifice with variable R or K acts as a *control valve*. The relation between P and Q is often found by measurement, but also can be computed using fluid finite-element software [6] or other computational fluid dynamics (CFD) software. As will be examined later in this chapter, the P–Q relation for hydraulic valves is important, because valves commonly serve in hydraulic actuators. Hydraulic units are listed in Appendix A.

The most common hydraulic fluid is oil, but other fluids such as water are sometimes used. Air is another popular fluid, but systems using it are called *pneumatic* systems. Because air is much more compressible than hydraulic liquids, thermodynamic effects can no longer be ignored. Thus pneumatic systems are usually more difficult to analyze than hydraulic systems. Also, pneumatic pressures are seldom as high as common hydraulic pressures, and thus pneumatics are not covered in this book. Both hydraulics and pneumatics are examples of *fluid power systems.*

16.3 MODELING HYDRAULIC CIRCUITS IN SPICE

The varieties of systems software examined in the preceding chapter can be applied to hydraulic and electrohydraulic systems. As that chapter discussed, systems software is often preferred to pure finite-element software. While the coupled finite elements in Chapter 14 solved electric circuits coupled to magnetics and then coupled to structural mechanics, adding coupling to hydraulic finite elements is very difficult. In fact, no papers can be found that attempt coupled electrohydraulic finite-element analysis, although a few couple electromagnetic finite elements with those for acoustics [7] or fluid flow [8].

Because one of the most common systems programs used by electrical engineers is SPICE (in commercial and free versions), it is here used to model hydraulic circuits. The electric circuits in SPICE can be used to model hydraulic circuits by the analogies of Table 16.1. For linear orifices, the ordinary constant resistor suffices. However, for

the nonlinear P–Q relation (16.3) of turbulent orifices, the electric circuit requires a resistor with a nonlinear V–I relation. Several versions of SPICE feature such a nonlinear resistor.

Example 16.1 SPICE Model of Hydraulic Circuit with Linear (Laminar) Orifices A hydraulic circuit containing two laminar orifices in parallel hydraulic lines is shown in Figure E16.1.1. The orifice hydraulic resistances are $R_1 = 1$ MPa s/m^3 and $R_2 = 2$ MPa s/m^3. They are both supplied by a pump of constant pressure $P_S = 5$ kPa. Find the flow rates in both orifices.

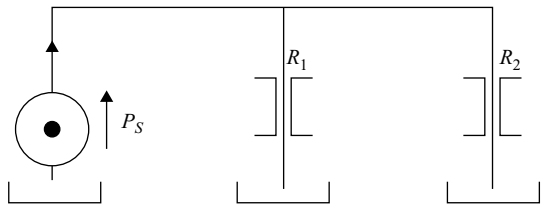

FIGURE E16.1.1 Hydraulic circuit with two parallel laminar orifices.

Solution The analogous SPICE electric circuit is shown in Figure E16.1.2. Since there are no capacitances and no inductances (neither hydraulic nor electric), the flows are DC. The computed values agree exactly with Ohm's law, being 5 mA in R_1 and 2.5 mA in R_2. Thus the flow rates are 5E–3 m^3/s and 2.5E–3 m^3/s, respectively.

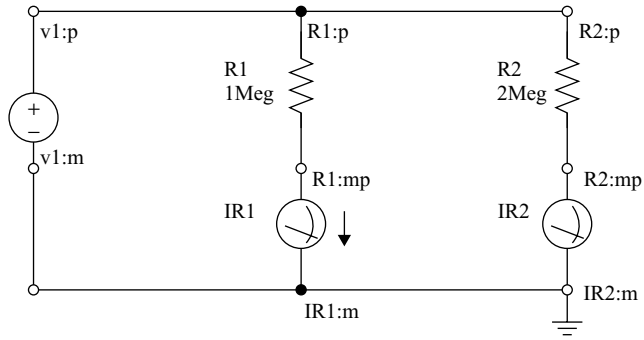

FIGURE E16.1.2 SPICE electric circuit model in Figure E16.1.1.

Example 16.2 SPICE Model of Hydraulic Circuit with Linear and Nonlinear (Turbulent) Orifices A hydraulic circuit containing a linear laminar orifice in series with a turbulent orifice is shown in Figure E16.2.1 [9,10]. The turbulent orifice has the constant K in its square law P–Q relation of Table 16.1. The laminar orifice has hydraulic resistance R. The given values are $K = 1$, $R = 1$, and source pressure $P_S = 1$ Pa. Find the DC flow rate Q.

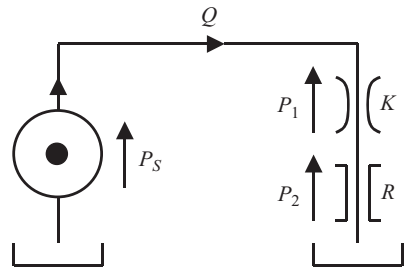

FIGURE E16.2.1 Hydraulic circuit with a turbulent orifice in series with a laminar orifice. Reprinted with permission from SAE Paper 2000-01-2633 © 2000 SAE International.

Solution Maxwell SPICE includes nonlinear resistors, indicated by the crooked line superimposed on the upper resistor in the model in Figure E16.2.2. The computed current is 0.618 A, which means that the computed flow rate $Q = 0.618$ m^3/s.

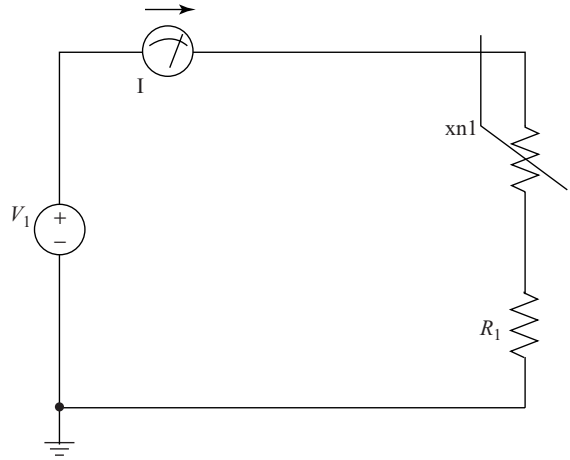

FIGURE E16.2.2 SPICE electric circuit model in Figure E16.2.1.

To verify the computed Q, the following method is used [11]. Applying Kirchhoff's voltage law to Figures E16.2.1 and E16.2.2,

$$P_S = P_1 + P_2 \tag{E16.2.1}$$

in which from (16.2) and (16.3):

$$P_1 = \frac{Q^2}{K^2}, \quad P_2 = QR \tag{E16.2.2}$$

Substituting (E16.2.2) into (E16.2.1) gives:

$$P_S = \frac{Q^2}{K^2} + RQ \tag{E16.2.3}$$

where Q is the unknown. Putting (E16.2.3) in quadratic form:

$$Q^2 + RK^2Q - K^2P_S = 0 \tag{E16.2.4}$$

Solving using the quadratic formula gives two roots [12]:

$$Q = -\frac{RK^2}{2} \pm \frac{1}{2}\sqrt{R^2K^4 + 4K^2P_S} \tag{E16.2.5}$$

Substituting the given unity values of R, K, and P_S gives $Q = +0.618$ and $Q = -1.618$. The negative value is impossible, and thus $Q = +0.618$ m^3/s, agreeing exactly with the SPICE computation.

Example 16.3 SPICE Model of Switched Hydraulic Circuit with Hydraulic Capacitance The hydraulic circuit shown in Figure E16.3.1 contains a manual valve "switch" that is thrown at time zero. Before time zero, all of the flow from the constant flow source Q is shunted through the valve to the tank "ground." At time zero, the valve sends the flow through the hydraulic components to the right, consisting of a laminar orifice with hydraulic capacitance. The values are $Q = 10$ m^3/s, $R = 100$ Pa s/m^3, and $C = 100$E–6 m^3/Pa. To be found is the hydraulic pressure as a function of time.

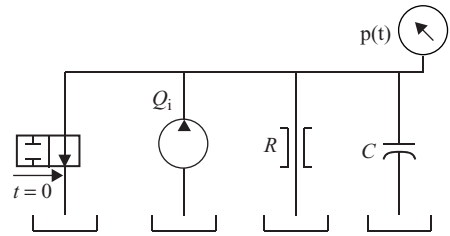

FIGURE E16.3.1 Hydraulic circuit with capacitance C, laminar resistance R, constant flow source Q_1 that is switched from tank at time zero. Reprinted with permission from SAE Paper 2000-01-2633 © 2000 SAE International.

Solution The analogous SPICE electric circuit model is shown in Figure E16.3.2. It consists of a current source of 10 A that is switched on at time zero, and a parallel 100-Ω resistor and 100-μF capacitor. Since the RC time constant is 0.01 s, the rise time of the pressure should be 0.01 s. The SPICE output voltage versus time is shown

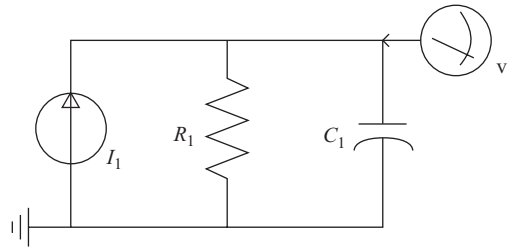

FIGURE E16.3.2 SPICE electric circuit model in Figure E16.3.1.

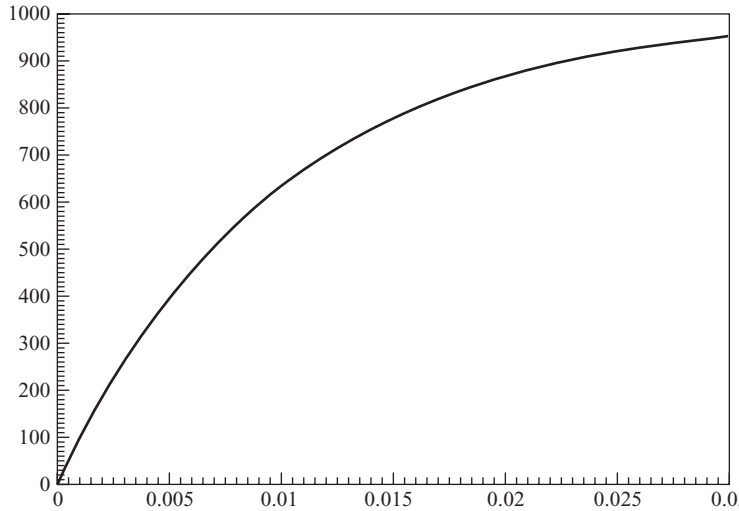

FIGURE E16.3.3 Voltage versus time (in seconds) computed by model in Figure E16.3.2.

in Figure E16.3.3. As expected, its time constant is 0.01 s. It approaches the final value of 1000 V, which equals the expected 10 A times 100 Ω. Thus the final steady-state pressure of the hydraulic circuit is 1000 Pa.

16.4 ELECTROHYDRAULIC MODELS IN SPICE AND SIMPLORER

SPICE hydraulic models can be combined with the SPICE electrical/magnetic/mechanical models of the preceding chapter to make electrohydraulic models. If desired, other electric circuit software such as Simplorer can be used instead of SPICE.

The simplest electrohydraulic models assume ideal proportional hydraulic *control valves*. Such valves produce fluid flow proportional to valve position regardless of pressure. An example familiar to everyone is a faucet that has flow rate directly proportional to its position x. If its position is zero, there is no flow, and the flow

rate is always approximately proportional to the position. In magnetic actuators, oftentimes the flow is directly through the "air" gap, and thus such actuators are often called *wet solenoids.* A dry alternative is to have the magnetic actuator armature push a rod through a physically separate proportional valve.

Such proportionality between position and flow rate is readily modeled using the *dependent sources* available in SPICE and Simplorer. SPICE includes the following four types of dependent sources identified by four letters.

- *E*, voltage-controlled voltage source with proportionality constant = (source voltage)/(controlling voltage at any node).
- *F*, current-controlled current source with proportionality constant = (source current)/(controlling current in any branch).
- *G*, voltage-controlled current source with proportionality constant = (source current)/(controlling voltage at any node).
- *H*, current-controlled voltage source with proportionality constant = (source voltage)/(controlling current in any branch).

Use of these dependent sources is shown in the SPICE electrohydraulic model in Figure 16.3 [10]. It is based on the Bessho magnetic actuator Maxwell SPICE model in Figure 15.1. Added to it are two dependent sources and other elements to model hydraulics. The hydraulic circuit is in the lower left corner of Figure 16.3, and consists of a linear orifice with $R = 1$ and the dependent source G_1. The flow source G_1 is set to 1000 m^3/(s m) and is dependent on the magnetic actuator airgap x. The second dependent source is G_2 added to the mechanical circuit on the right. G_2 is set to 1 N/Pa and is a flow force proportional to the flow in the hydraulic valve. The assumed proportionality of sources G_1 and G_2 is usually only approximately obeyed in actual hydraulic valves; the next section will discuss more realistic valve and hydraulic system models.

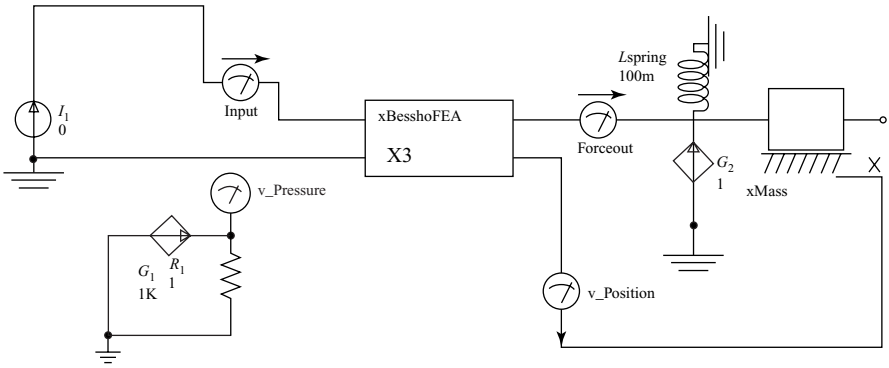

FIGURE 16.3 Maxwell SPICE model of simple electrohydraulic system with Bessho actuator driving a proportional control valve. Reprinted with permission from SAE Paper 2000-01-2633 © 2000 SAE International.

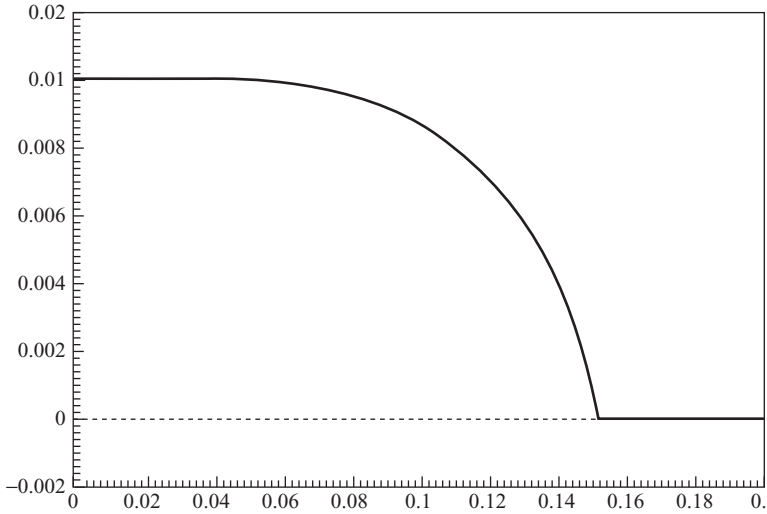

FIGURE 16.4 Computed magnetic actuator armature position in m (y axis) versus time in s for electrohydraulic system of Figure 16.3. Reprinted with permission from SAE Paper 2000-01-2633 © 2000 SAE International.

The computed Bessho actuator armature position versus time for Figure 16.3 is plotted [10] in Figure 16.4. Compared to the plot of Figure 15.3 (curve 1), the closure time has increased from 99 to 150 ms. The hydraulic force has caused the armature to move more slowly.

The next SPICE model has the linear orifice of Figure 16.3 replaced by a nonlinear orifice with $K = 3$. The computed armature closure time increases to 160 ms. Next, a hydraulic capacitance $C = 0.1$ is added in parallel with the nonlinear orifice, and the computed closure time changes to 106 ms. The capacitance reduces the hydraulic force acting on the valve, thereby increasing the speed of armature motion.

Another SPICE model was made of the Bessho magnetic actuator driven by a pulse-width modulated (PWM) voltage of the type presented in Chapter 7. The electronic chopper circuit creating the PWM voltage is in the upper left of Figure 16.5, which also contains the electrohydraulic SPICE model in Figure 16.3. Note that the chopper circuit contains a dependent switch which is governed by the V_3 voltage source that has a frequency of 100 Hz. The chopper circuit also contains a "*flyback" diode* so that when the 50-V DC source is switched off, the inductive current of the magnetic actuator can flow to ground rather than cause arcing in the switch. The electronic switch is typically a semiconductor chip such as an SCR or IGBT. The resulting PWM voltage computed by SPICE is shown in Figure 16.6 for a duty cycle of 50%. Thus the DC chopper voltage is 50% of the input 50, or 25 V.

The computed input current shown in Figure 16.7 consists of the previous rising exponential with a dip caused by the moving armature, but also it has a ripple superimposed. The ripple is at the 100-Hz chopper frequency. The resulting magnetic

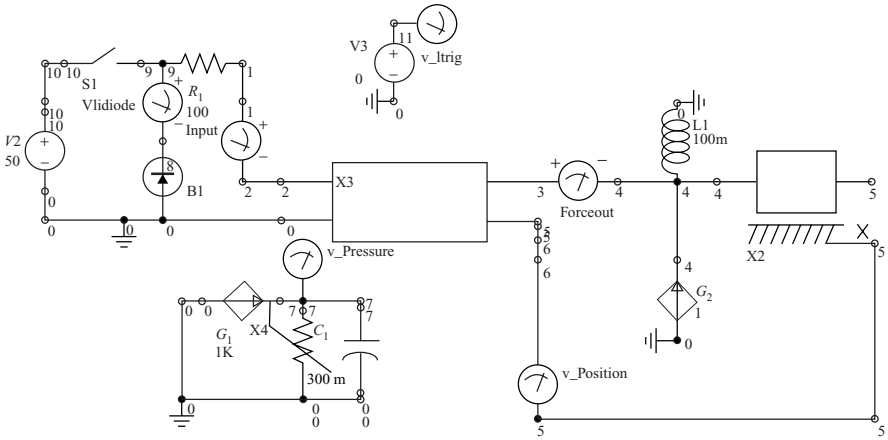

FIGURE 16.5 Chopper-driven PWM magnetic actuator in an electrohydraulic system modeled in SPICE. The chopper circuit is in the upper left, driving the Bessho actuator represented by the block-labeled X_3.

force is shown in Figure 16.8 and also contains a ripple. The computed magnetic actuator armature airgap versus time is shown in Figure 16.9; note that closure takes about 140 ms, similar to Figure 16.4. The computed hydraulic pressure and flow rate are shown in Figures 16.10 and 16.11, respectively. Since the flow rate is assumed proportional to armature position (which is 10 mm minus the airgap), the flow rate increases with time [12].

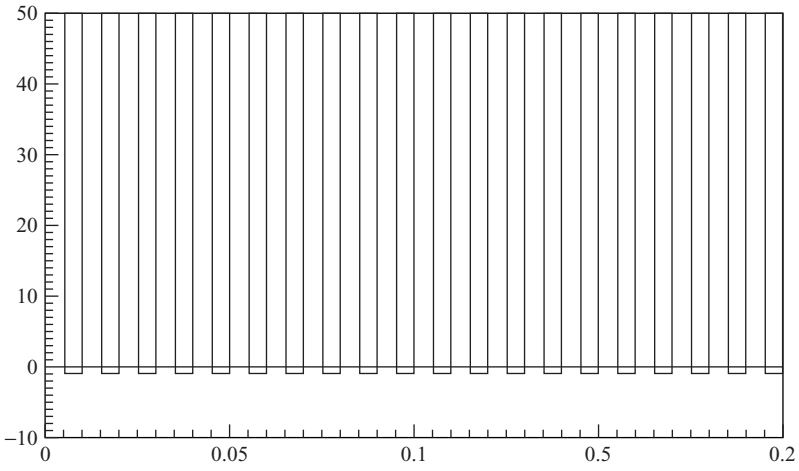

FIGURE 16.6 Computed PWM voltage (V along *y* axis) versus time (s) produced by chopper of Figure 16.5.

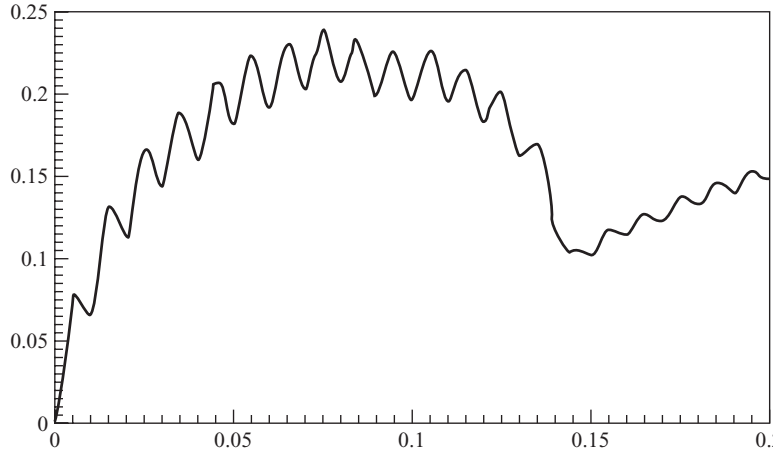

FIGURE 16.7 Computed magnetic actuator current (A on *y* axis) versus time (s) for Figure 16.5.

A hydraulics library is available for Simplorer. One of its hydraulic elements, the variable orifice, is used here to model a control valve operated by the Bessho magnetic actuator. The variable orifice is labeled as *RHYD*1 in the Simplorer model in Figure 16.12, which also contains a Simplorer fixed orifice with $R = 1E9$ Pa s/m^3. To achieve faster performance than the previous electrohydraulic systems of Figures 16.4–16.11, the 0.5-A current is turned on instantly (with 0 rather than 20 ms rise time) and the moving mass is reduced from 6 to 1.4 kg. The resulting armature position versus time computed by Simplorer is shown in Figure 16.13 assuming no

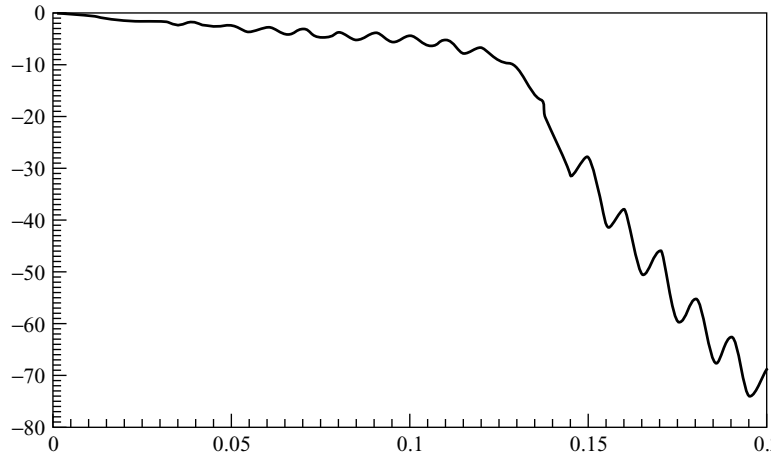

FIGURE 16.8 Computed magnetic force (N on *y* axis) versus time (s) for Figure 16.5.

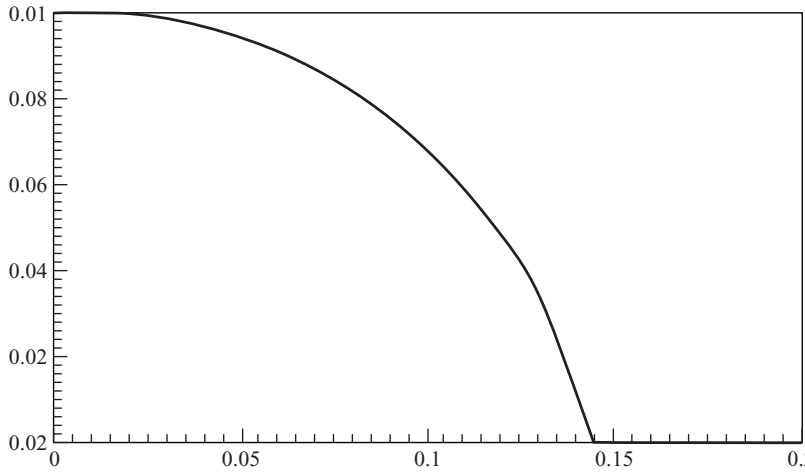

FIGURE 16.9 Computed magnetic armature position (m on *y* axis) versus time (s) for Figure 16.5.

flow forces. As expected, movement is now much faster, closing in only 34 ms. The pressure source of 1 MPa (10 bar) then produces the flow rate also graphed in Figure 16.13 for wet flow through the airgap that ceases upon its closure.

The Simplorer hydraulic orifice also allows flow forces to be included. For a flow force factor of 10 on the variable orifice, the computed results are graphed in Figure 16.14. Compared with Figure 16.13, the armature now closes in 31.5 ms, which is 2.5 ms faster.

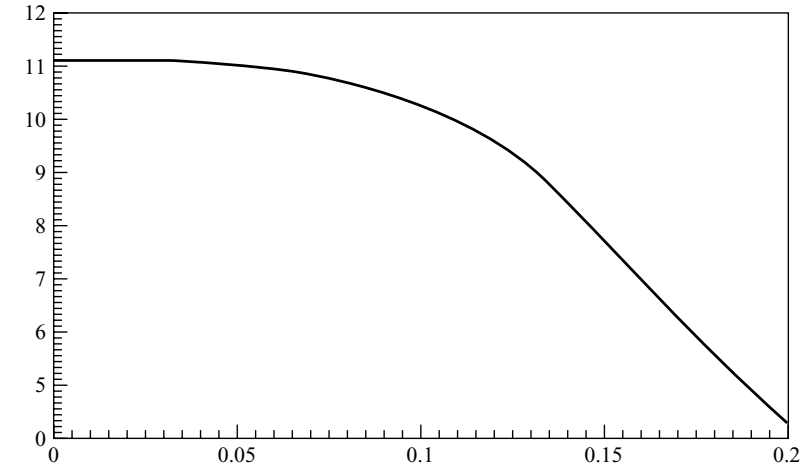

FIGURE 16.10 Computed hydraulic pressure (Pa on *y* axis) versus time (s) for Figure 16.5.

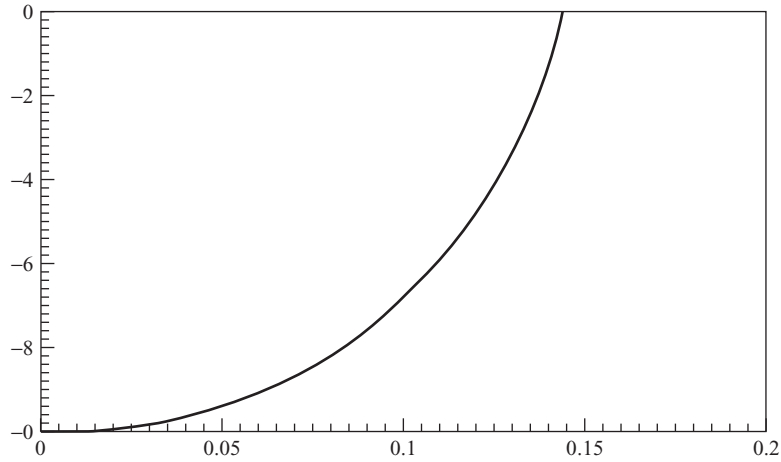

FIGURE 16.11 Computed hydraulic flow rate (m^3/s on *y* axis) versus time (s) for Figure 16.5.

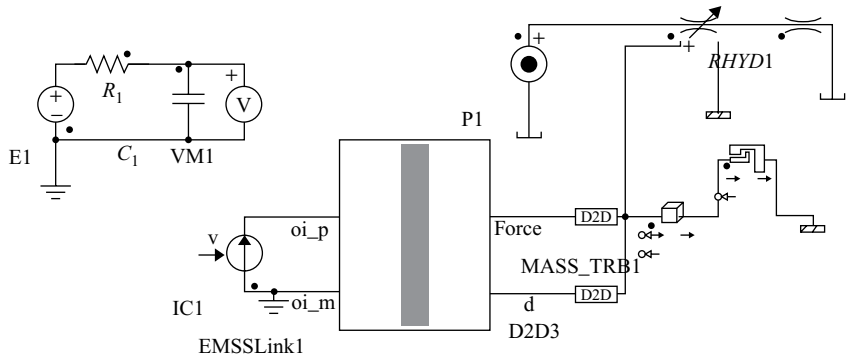

FIGURE 16.12 Simplorer model of Bessho magnetic actuator in an electrohydraulic system containing the variable orifice *RHYD*1. To its right is the fixed orifice with R = 1E–9 m^3/(s Pa).

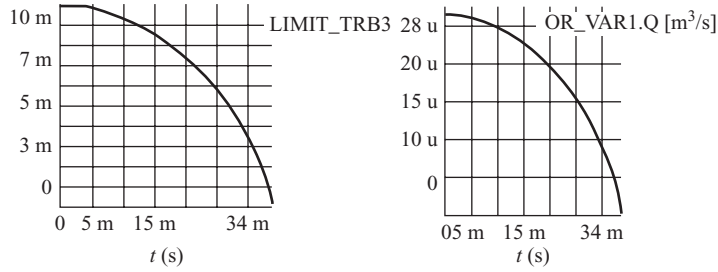

FIGURE 16.13 Computed results for Figure 16.12 with no flow forces. The left graph is armature airgap (m) versus time (s). The right graph is the flow rate (m^3/s) versus time (s).

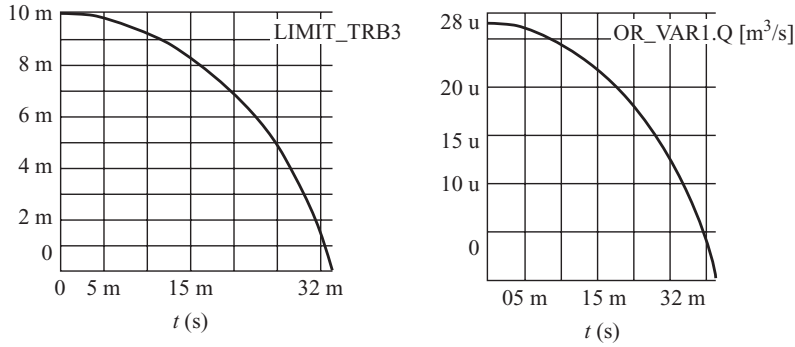

FIGURE 16.14 Computed results for Figure 16.12 with valve *RHYD1* flow force factor of 10. The left graph is armature airgap (m) versus time (s). The right graph is the flow rate (m^3/s) versus time (s).

16.5 HYDRAULIC VALVES AND CYLINDERS IN SYSTEMS MODELS

16.5.1 Valves and Cylinders

The most common hydraulic actuator is the hydraulic cylinder, which contains a piston operated by hydraulic pressure. The cross-section of a hydraulic cylinder placed in a typical electrohydraulic system is shown in Figure 16.15. The differential pressure P between the two sides of the piston of area A creates the hydraulic force. Hydraulic cylinders are easily visible on many tractors, dozers, power shovels, dump trucks, garbage trucks, snowplows, vertical lift bridges, etc.

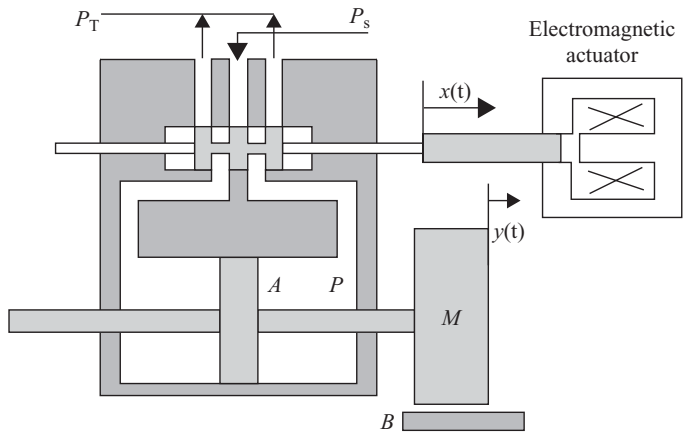

FIGURE 16.15 Electrohydraulic system containing a magnetic actuator driving a control valve that operates a hydraulic cylinder with moving mass *M*.

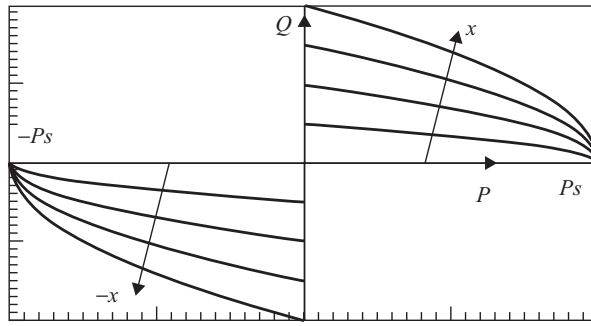

FIGURE 16.16 Typical pressure versus flow rate curves of a control valve. P is the pressure to the load and Q is the flow rate to the load. The valve spool position x is zero when the valve is closed and Q is zero.

If the cylinder position is y as shown in Figure 16.15, then the flow rate (in cubic meters per second) must obey:

$$Q = A\,dy/dt \tag{16.4}$$

The electrohydraulic system of Figure 16.15 also shows the cross section of a typical control valve [1] driven by a magnetic actuator. The armature of the magnetic actuator is directly connected to the *valve spool*, the movable part of the valve that is shaped like a spool for thread. The spool in Figure 16.15 has three *lands,* which are large diameter cylindrically shaped regions. The valve in Figure 16.15 is called a *four-way valve* because it has a total of four flow paths [13, 14]. Its two hydraulic inputs are tank pressure P_T and supply pressure P_S.

The input–output characteristics of the valve are those shown in the typical family of curves in Figure 16.16. Each curve is a plot of output (load) pressure P versus flow rate to the load Q. The valve position x is zero when closed and can be moved in either the positive and negative direction in Figure 16.15. The flow rate curves of Figure 16.16 are usually approximated by the equation [13]:

$$Q = K_V x\sqrt{P_S - P} \tag{16.5}$$

where K_V is called the valve coefficient and the tank pressure has been assumed zero.

Since (16.5) is nonlinear with load pressure P, it is often linearized to allow easier analysis. Over a small range, the commonly assumed linear relation is:

$$Q = K_x x - K_p P \tag{16.6}$$

Note that if K_p is zero, then the valve is the ideal proportional valve assumed in the preceding section. This section, however, is more realistic in allowing K_p to be nonzero in the following derivations.

16.5.2 Use in SPICE Systems Models

The above valve and cylinder can be modeled in SPICE based on the linearized valve equation (16.6), the hydraulic cylinder equation (16.4), and Newton's laws. For the cylinder load mass M and damping B shown in Figure 16.15, the force balance equation is:

$$PA = B(dy/dt) + M(d^2y/dt^2) \tag{16.7}$$

To model (16.4), (16.6), and (16.7) in SPICE, they can be written as three simultaneous equations in Q, P, and y:

$$(1)Q + (K_p)P + (0)y = K_x x \tag{16.8}$$

$$(1)Q + (0)P - A\,dy/dt = 0 \tag{16.9}$$

$$(-B/A)Q + (A)P - M\,d^2y/dt^2 = 0 \tag{16.10}$$

The above three simultaneous differential equations are here simulated using three circuit meshes in SPICE. The three meshes appear in the bottom of the SPICE schematic of Figure 16.17. The upper portion of Figure 16.17 is the same as the previous SPICE electrical/magnetic/mechanical model of the Bessho magnetic actuator of Figure 15.1. As before, the block-labeled X_3 contains results of parametric magnetic finite-element analyses of the Bessho magnetic actuator.

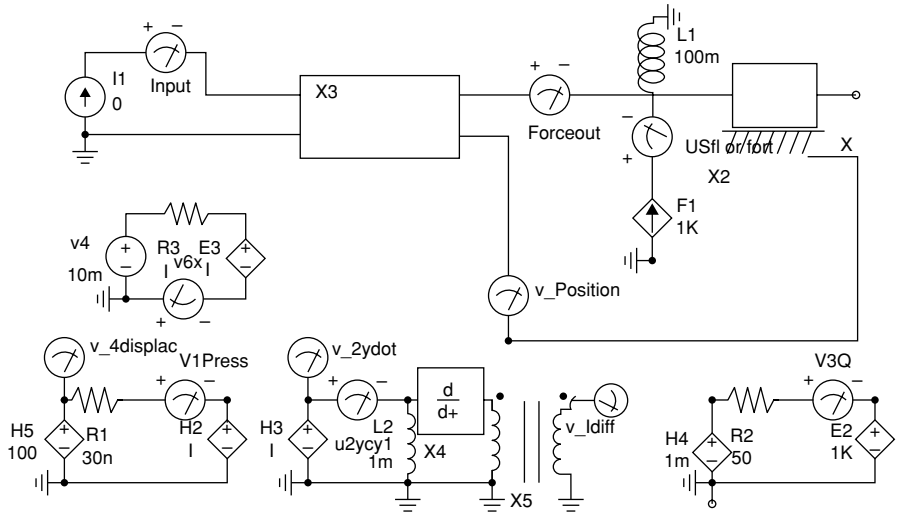

FIGURE 16.17 SPICE schematic of electrohydraulic system of Figure 16.15. The upper right armature mass is 6 kg. The upper left current source rises to 0.5 A with a time constant of 20 ms.

The lower left circuit mesh in Figure 16.17 represents (16.8). P is its mesh current to be computed. Its resistor is K_p. Its two dependent sources are related to the other two terms of (16.8). The left-hand-dependent H (current-controlled voltage) source is K_x times the armature position x. Its right–hand-dependent H (current-controlled voltage) source is equal to flow rate Q. Thus according to Kirchhoff's voltage law, this circuit mesh simulates (16.8).

The middle circuit mesh in the bottom of Figure 16.17 represents (16.9). Its mesh current is the cylinder position y to be computed. The inductor is of value A, and thus its voltage is $A(dy/dt)$. This voltage equals that of the dependent H (current-controlled voltage) source equal to Q according to Kirchhoff's voltage law. A differentiator is added to produce an additional voltage $A(d^2y/dt^2)$, which is transformed by an added ideal transformer to (d^2y/dt^2) for use elsewhere.

The lower right circuit mesh in Figure 16.17 represents (16.10). Its mesh current is the flow rate Q to be computed. The resistor is of value B/A. The left-hand-dependent H (current-controlled voltage) source is set to A times the pressure P. Its right-hand-dependent E (voltage-controlled voltage) source is set to $M(d^2y/dt^2)$, where (d^2y/dt^2) is found from the lower middle mesh.

To model the flow forces, the dependent F (current-controlled current) source is placed in the mechanical circuit in the upper right-hand corner of Figure 16.17. The flow force acting on the magnetic armature and valve spool is generally a nonlinear function of flow rate Q and position x, but is here modeled (as commonly done [14]) as a force proportional to Q directed to oppose the valve opening.

Thus the SPICE model in Figure 16.17 couples the solutions of electric currents, magnetic forces, flux linkages, hydraulic pressures and flow rates, and mechanical armature and cylinder motions, all together into one simultaneous solution [1].

The performance of the system model in Figure 16.17 was computed for a typical set of electrical, magnetic, hydraulic, and mechanical parameters. The electrical and magnetic parameters are those of the previously analyzed Bessho solenoid, and the hydraulic and mechanical parameters are labeled in Figure 16.17, including $A =$ 1.E–3 m^2, $B = 50A$, $K_x = 100$, and $K_p = 30.E{-}9$. The input current is assumed to rise to its rated 0.5 A with a 20 ms rise time, and the armature mass is 6 kg. For a load mass M (of Figure 16.16) set to 10 kg and then to 1000 kg, some computed results are in Figures 16.18–16.21.

Figure 16.18 shows that the flow rate Q is much higher for the light load M than for the heavy load. This dependence agrees with the governing equations (16.8)–(16.10).

Figure 16.19 shows that the armature position x of the magnetic actuator changes more slowly with the light load M. This slowdown is caused by the high flow rate of Figure 16.18 and the associated high flow force acting on the armature. When the flow rate is low, the flow force is also low. The low flow force is much smaller than magnetic force and thus the time to stroke is approximately 100 ms, the same as previously computed in Chapter 15 without any hydraulic force.

Figure 16.20 shows that the position y of the mass M changes much more slowly with the heavy mass than with the light mass, as expected from Newton's law of (16.7).

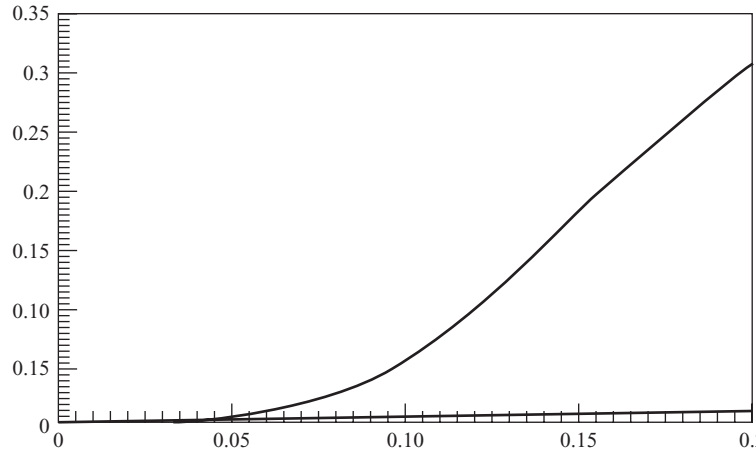

FIGURE 16.18 Computed Q (m^3/s on y axis) versus time (s) for electrohydraulic model in Figure 16.17. The upper curve is for $M = 10$ kg and the lower curve is for $M = 1000$ kg.

Finally, Figure 16.21 shows that the differential pressure P for both light and heavy values of M peaks at about 330.E5 Pa = 330 bar, a much higher pressure than magnetic pressures of less than 20 bar. Multiplying by $A = 1.E{-}3$ m^2, the peak hydraulic force is a respectable 33 kN.

The electrohydraulic system can next be modeled when chopper driven. The chopper is shown in the upper left corner of the SPICE model in Figure 16.22, and is similar to that of Figure 16.5. Note that the DC supply voltage is now 42 V, a standard voltage proposed for automobiles. The duty cycle is again 50%, and thus the output of

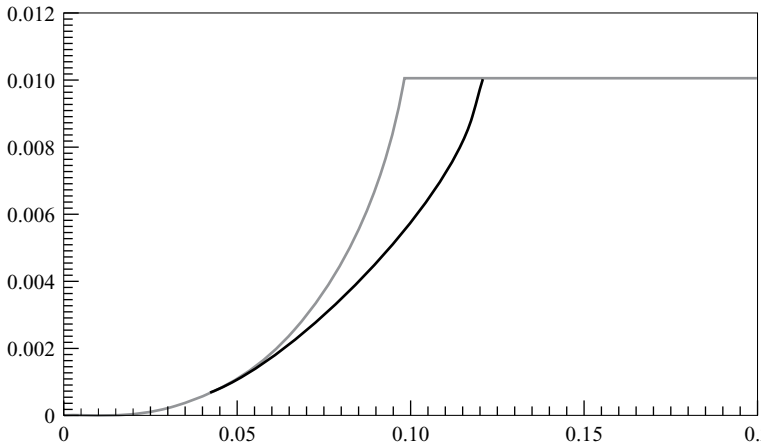

FIGURE 16.19 Computed magnetic armature position x (m along vertical axis) versus time (s) for electrohydraulic model in Figure 16.17. The right curve is for $M = 10$ kg and the left curve is for $M = 1000$ kg.

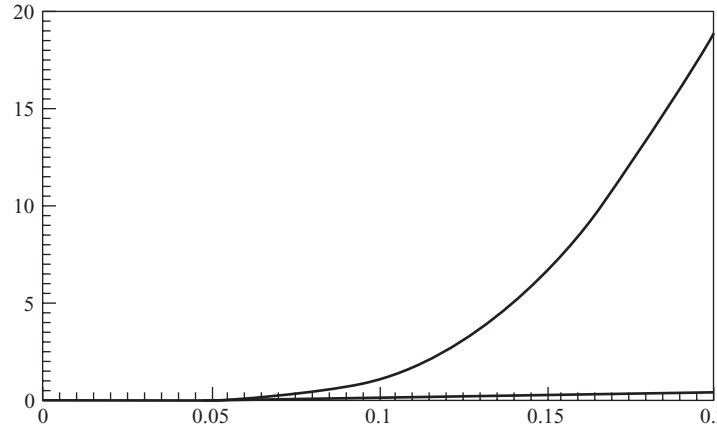

FIGURE 16.20 Computed cylinder position y (m on vertical axis) versus time (s) for electrohydraulic model in Figure 16.17. The upper curve is for $M = 10$ kg and the lower curve is for $M = 1000$ kg.

the chopper has 21 V DC. Figure 16.22 shows the computed current waveforms in the coil of the magnetic actuator. For both load mass values, the currents of Figure 16.22 show the 100-Hz chop rate superimposed on an *LR* circuit rise time, as expected. The currents of Figure 16.23 also exhibit the expected dip due to back voltage induced by motion that stops when the armature reaches its full 10-mm stroke. Figure 16.24 shows the computed armature position x. The armature moves its full 10 mm in 0.16 s for $M = 1000$ kg, but takes 0.19 s for $M = 10$ kg. The slowdown is caused by the high flow rate for the light mass, similar to the case without the chopper drive. Curves of

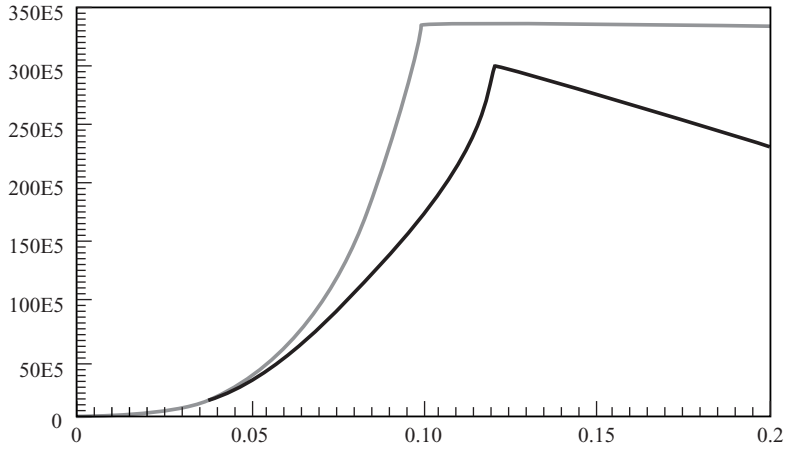

FIGURE 16.21 Computed differential pressure P (Pa on vertical axis) versus time (s) for electrohydraulic model in Figure 16.17. The lower curve is for $M = 10$ kg and the upper curve is for $M = 1000$ kg.

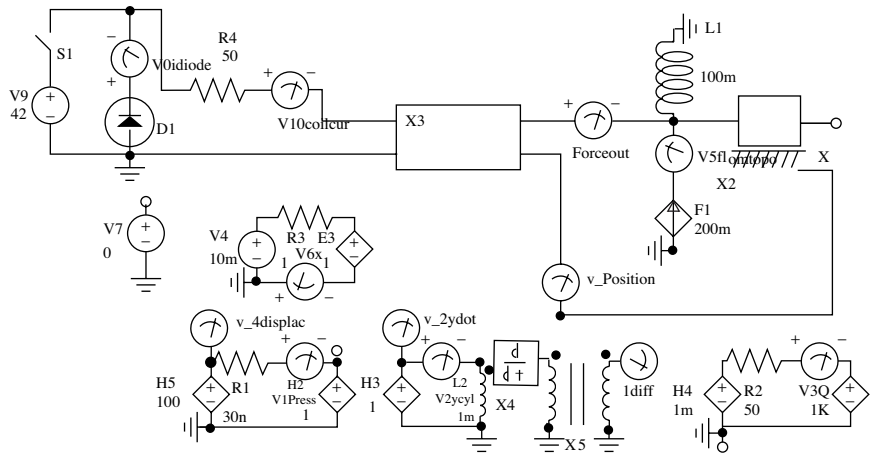

FIGURE 16.22 SPICE schematic of Figure 16.17 with added chopper drive in upper left corner. Reprinted with permission from SAE Paper OH 2002-01-1346 © 2002 SAE International and NFPA.

pressure and flow have also been obtained [15] that are qualitatively similar to those shown for the system without chopper drive.

While no magnetic sensor is shown in the electrohydraulic systems of Figures 16.15 and 16.22, oftentimes magnetic sensors are used. To determine the cylinder position, the magnetostrictive and linear variable differential transformer (LVDT) sensors of Chapter 11 are commonly employed, especially in feedback control systems. Also, to measure hydraulic flow rates, steel paddle wheels are occasionally placed

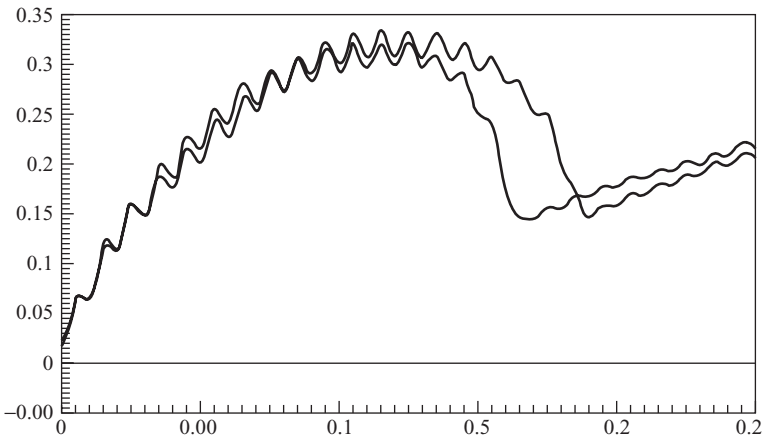

FIGURE 16.23 Computed coil current (A on *y* axis) versus time (s) for model in Figure 16.22. For $M = 10$ kg the current dips at 0.19 s, while for $M = 1000$ kg the current dips at 0.16 s. Reprinted with permission from SAE Paper OH 2002-01-1346 © 2002 SAE International and NFPA.

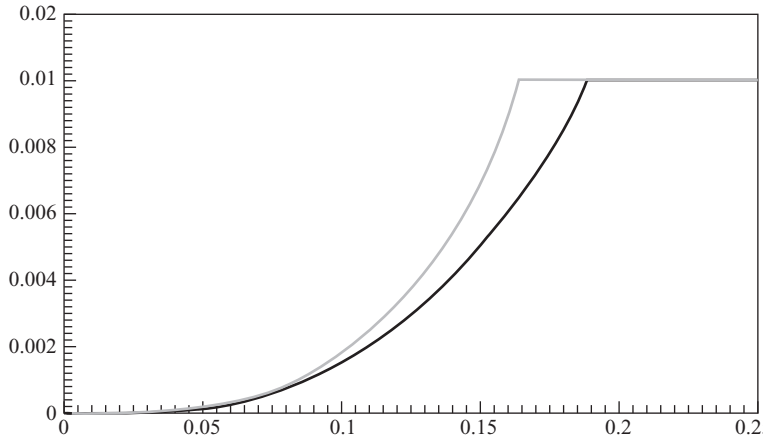

FIGURE 16.24 Computed armature position x (m on vertical axis) versus time (s) for model in Figure 16.22. The left curve is for $M = 1000$ kg, while the right curve is for $M = 10$ kg. Reprinted with permission from SAE Paper OH 2002-01-1346 © 2002 SAE International and NFPA.

in hydraulic lines; the passing steel paddles behave similarly to the gear teeth of the Hall sensors of Chapter 10. Such *flowmeters* can also use the inductive pickup coils discussed in Chapter 11.

16.6 MAGNETIC DIFFUSION RESISTOR IN ELECTROHYDRAULIC MODELS

To include the effects of eddy currents in electrohydraulic systems models, one can use the eddy current diffusion resistor introduced in Chapter 15 [16]. As described in Section 15.4, this parallel resistor varies in value with magnetic saturation. Its values were calculated for the Bessho magnetic actuator and will be used here. For the nominal 0.5-A current in the Bessho actuator, the nonlinear eddy current diffusion resistor was computed to be $R_{EN} = 1320\ \Omega$.

Adding this parallel resistor to the Simplorer electrohydraulic model in Figure 16.12, the new output is shown in Figure 16.25. With no flow force, both the armature position and the flow rate graphs show that the armature now closes in 40 ms, which is 18% longer than the 34 ms of Figure 16.13. This time delay due to eddy current diffusion can be a problem in automotive fuel injectors and other electrohydraulic systems with models similar to Figure 16.12. At high engine speeds, fuel injectors often must open or close in less than 1 ms.

The same eddy current diffusion resistor $R_{EN} = 1320\ \Omega$ is added to the electrohydraulic system with Bessho magnetic actuator and the hydraulic cylinder of Figure 16.15. The new SPICE model is shown in Figure 16.26, which has a step input current of 0.5 A and cylinder load mass of 1000 kg [17]. It has a lighter armature mass of 1.4 kg than the previous model in Figure 16.17, as well as a higher $K_x = 3000$.

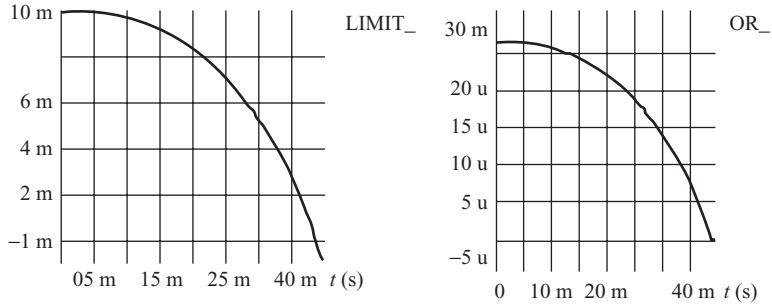

FIGURE 16.25 Computed results for Simplorer model in Figure 16.12 with added parallel resistor of 1320 Ω and with no flow forces. The left graph is armature airgap (m) versus time (s). The right graph is the flow rate (m^3/s) versus time (s).

Computed results are shown with and without the 1320-Ω eddy resistor in Figures 16.27–16.31. Figure 16.27 plots armature position and Figure 16.28 shows armature magnetic force. Note that the step current and lighter armature mass cause the airgap to close much faster than 100 ms, as expected. Hydraulic pressure and flow rate are shown in Figures 16.29 and 16.30, respectively. Multiplying the peak pressure by cylinder area $A = 1.E{-}3\ m^2$, the peak hydraulic force is a respectable 30 kN. Finally, Figure 16.31 plots the cylinder load position versus time. All of the computed results show that eddy currents produce significant delays in the electrohydraulic system response [17].

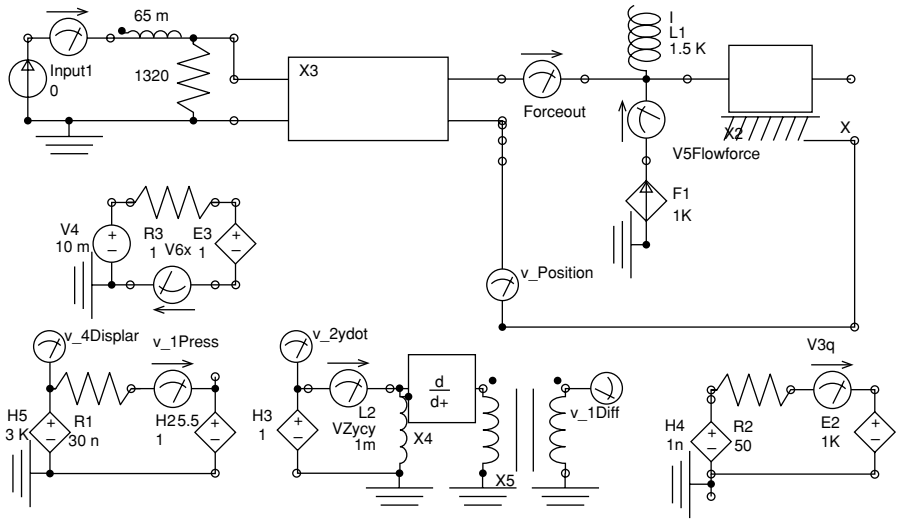

FIGURE 16.26 SPICE model of electrohydraulic system with hydraulic cylinder of Figure 16.15 with added diffusion resistor of 1320 Ω. The upper right armature mass is 1.4 kg. The upper left current source steps instantly to 0.5 A.

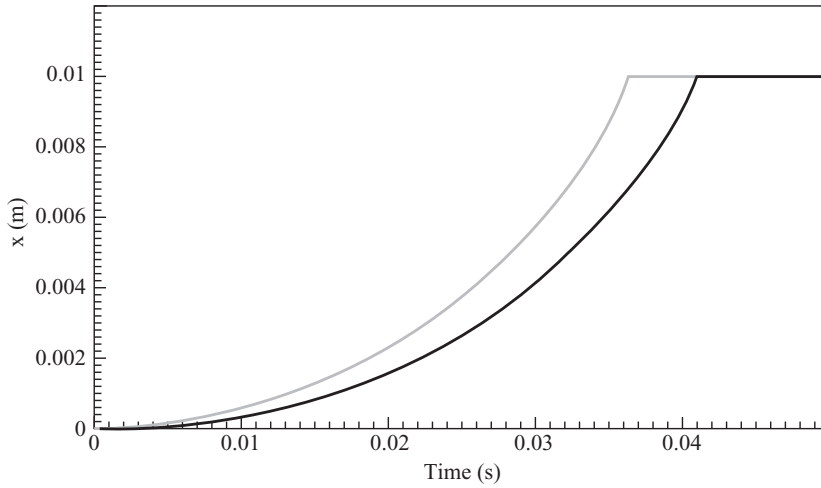

FIGURE 16.27 Computed armature position x (m) versus time for Figure 16.26. The left curve is without a nonlinear diffusion resistor, while the right curve is with a parallel 1320-Ω resistor.

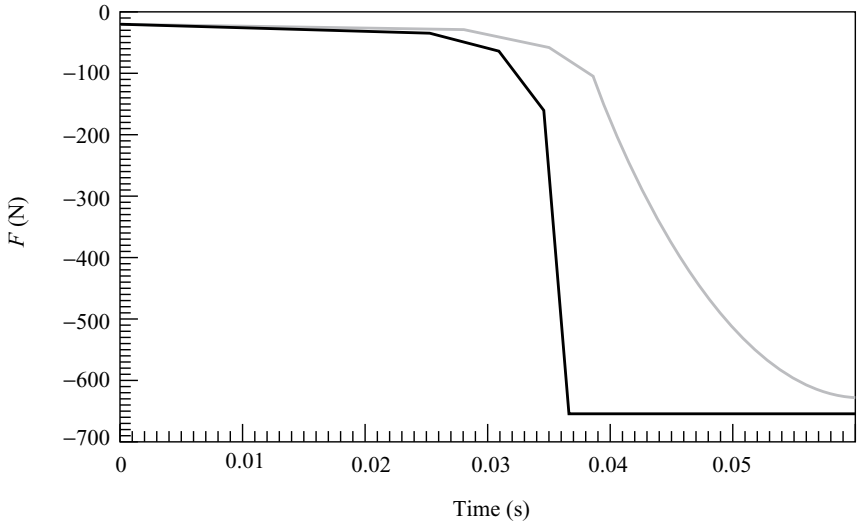

FIGURE 16.28 Computed magnetic force (N) versus time for Figure 16.26. The left curve is without a nonlinear diffusion resistor, while the right curve is with a parallel 1320-Ω resistor.

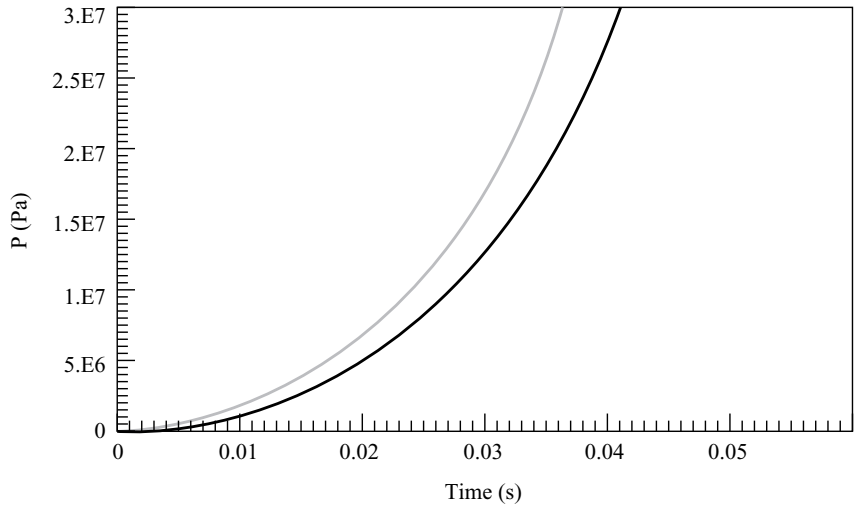

FIGURE 16.29 Computed hydraulic pressure (Pa) versus time for Figure 16.26. The left curve is without a nonlinear diffusion resistor, while the right curve is with a parallel 1320-Ω resistor.

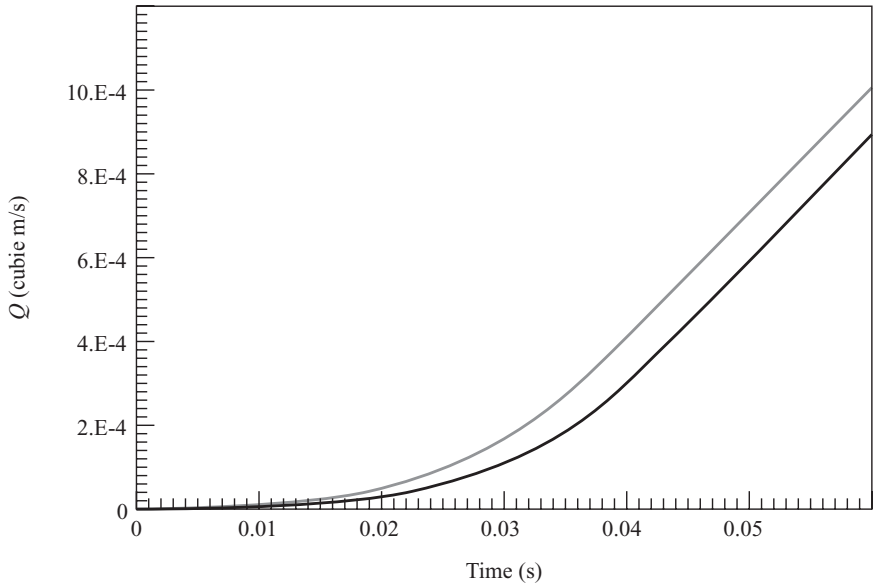

FIGURE 16.30 Computed flow rate (m^3/s) versus time for Figure 16.26. The left curve is without a nonlinear diffusion resistor, while the right curve is with a parallel 1320-Ω resistor.

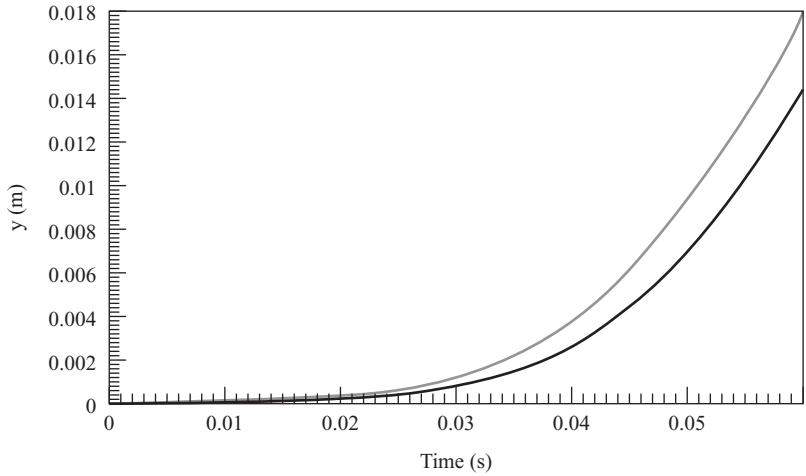

FIGURE 16.31 Computed cylinder position y versus time for Figure 16.26. The left curve is without a nonlinear diffusion resistor, while the right curve is with a parallel 1320-Ω resistor.

16.7 OPTIMIZATION OF AN ELECTROHYDRAULIC SYSTEM

The three dimensional (3D) magnetic solenoid actuator analyzed in Section 15.6.2 is used to drive a hydraulic valve, and the entire electrohydraulic system needs to be optimized. The system is shown schematically in Figure 16.32. Here the cosimulation of the coupled electrical, magnetic, mechanical, and hydraulic systems is achieved by cosimulation at each time step between Maxwell and Simplorer software [18].

In Maxwell, an external transient to transient link is specified with Simplorer. Then within Simplorer, a finite-element subcircuit is added and linked to the Maxwell finite-element model. The computed system performance includes all eddy current effects within the two dimensional (2D) or 3D magnetic actuator, as well as all mechanical and hydraulic forces and parameters. No diffusion resistor needs to be added.

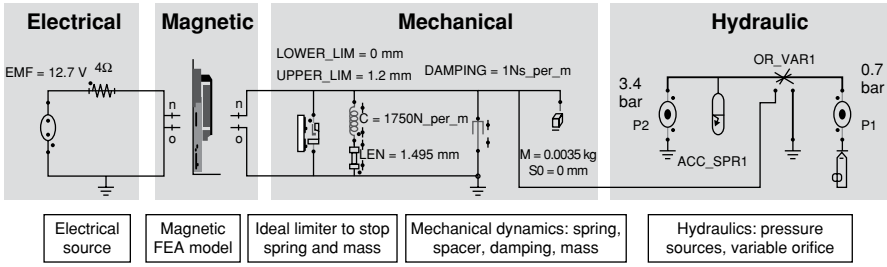

FIGURE 16.32 Schematic of time-by-step cosimulation of electrical, magnetic, mechanical, and hydraulic systems for a solenoid operating a hydraulic valve. Published with permission of TRW Automotive and ANSYS, Inc.

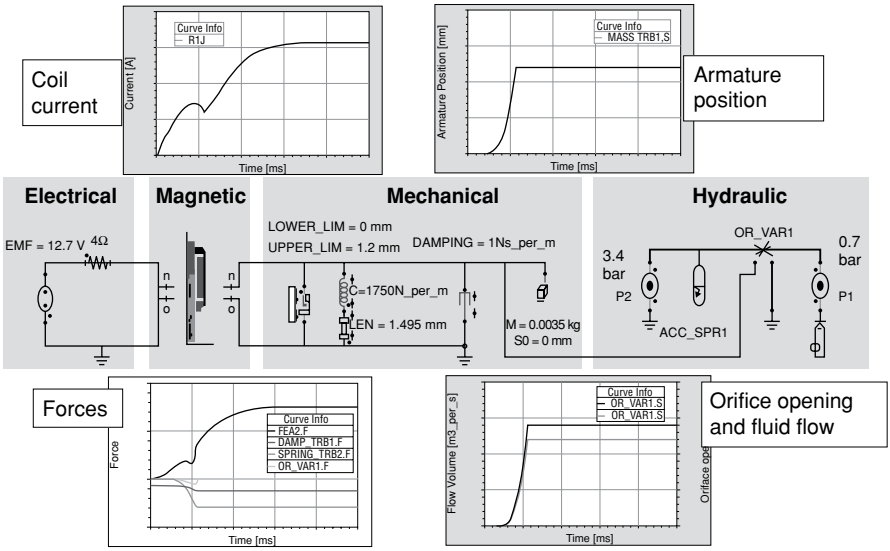

FIGURE 16.33 Computed results for the electrohydraulic system of Fig. 16.32, showing waveforms of current, position, various forces, and hydraulic flow rate. Published with permission of TRW Automotive and ANSYS, Inc.

The computed electrohydraulic system results are summarized in Figure 16.33. The computed coil current waveform shows the expected dip at closing and then rises to its final DC value. The armature position versus time display verifies the closing time of the current waveform. The force curves displayed include magnetic, mechanical, and hydraulic forces. Finally, the flow versus time curve shows the hydraulic flow rate as the valve orifice closes. The engineer can determine the effects of any electrical, magnetic, mechanical, or hydraulic design change on the system performance and thereby optimize the electrohydraulic system performance.

16.8 MAGNETIC ACTUATORS FOR DIGITAL HYDRAULICS

Instead of the valves discussed so far in this chapter, which can be called analog or servo valves, one can use more recently developed *digital valves.* Digital valves are less prone to faults (such as due to hydraulic fluid impurities) and can be less complex and thus less expensive [19].

Digital hydraulics includes digital valves, pumps, and cylinders. Digital valves have on/off or binary operation and are often placed in parallel in valve packages with each valve sized differently (such as 1, 2, 4, 8 etc. for binary control).

Digital hydraulics can be safer and more energy efficient than conventional analog hydraulics. For example, digital hydraulics can theoretically unload a railcar full of logs or coal with zero net power consumption.

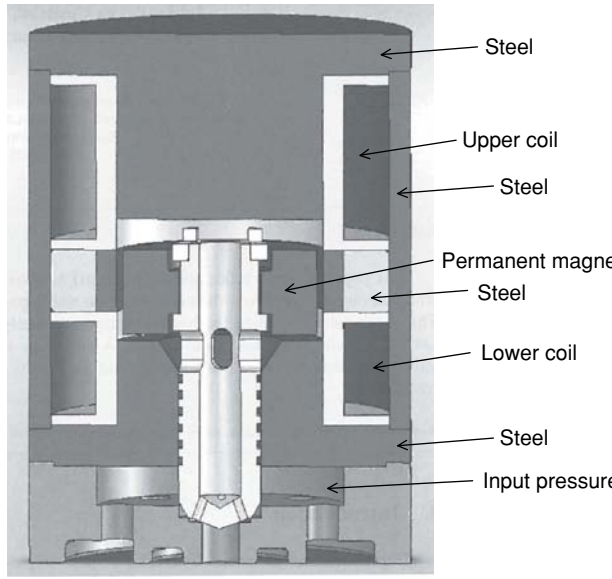

FIGURE 16.34 Digital hydraulic hammer valve with radially magnetized permanent magnet armature. Reprinted by permission from *Int J Fluid Power* [20].

The on/off valve is the key to digital hydraulics, and is most commonly operated by a magnetic solenoid actuator. Since many such on/off valves are usually required, it is necessary to reduce the size and power consumption of each solenoid actuator and its valve. A solenoid valve design developed for digital hydraulics is shown in Figure 16.34. It has an upper coil, a lower coil, and a radially magnetized permanent magnet armature, all forming a variation of the design of Figure 7.4. Called a hammer actuator, the hydraulic fluid flow around the valve input is designed to be compatible with the magnetic circuit design. This magnetic actuator is called *bistable* because it has two stable positions which are reversed by a short current pulse [20, 21]. The computed magnetic flux density in the actuator is shown in Figure 16.35 for both no coil current and for a current pulse in a coil. A typical hammer valve size is roughly that of a common 9-V battery [20].

For a typical voltage pulse swinging between $+24$ V and -24 V, the current waveform at a typical drive frequency is plotted in Figure 16.36. Note the good agreement between computed and measured current waveforms. For a higher drive frequency of 200 Hz (the maximum), Figure 16.37 plots both the voltage and pressure difference waveforms. The measured response time of the hammer valve was about 2.5 ms [20]. For a supply pressure of 210 bar, Figure 16.38 plots the measured pressure difference versus flow rate curve.

After prototyping the single hammer valve, 16 such valves were incorporated into a digital valve package [19,21]. With all valves in parallel, the package has 17 possible discrete flow states. There is a large number of possible valve combinations for most of the 17 flow states. Future valve packages containing more valves would enable more precise flow control.

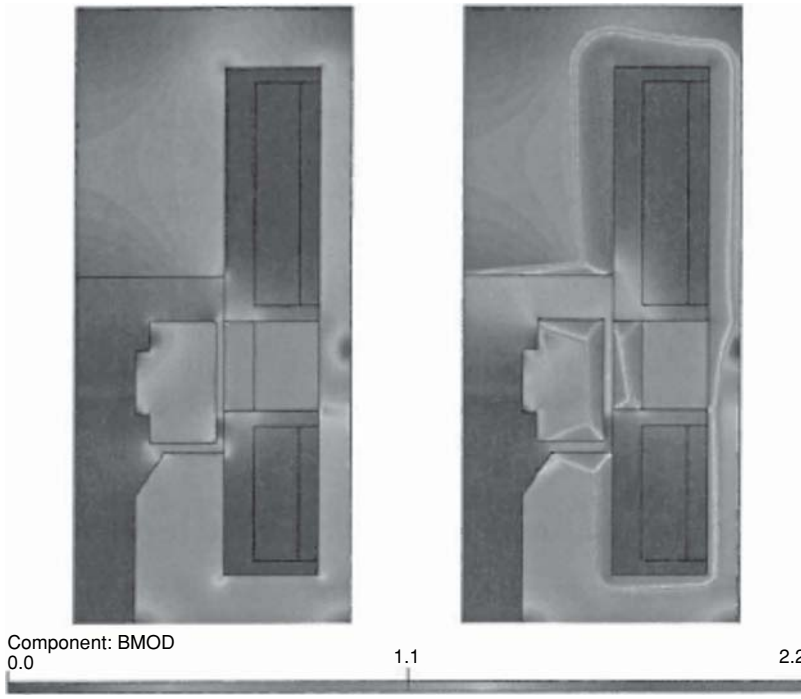

FIGURE 16.35 Flux densities (T) computed in actuator of Figure 16.34. The left display is for no coil current with the valve closed, while a coil is fed an opening current pulse in the right display (note the visible skin effects). Reprinted by permission from *Int J Fluid Power* [20].

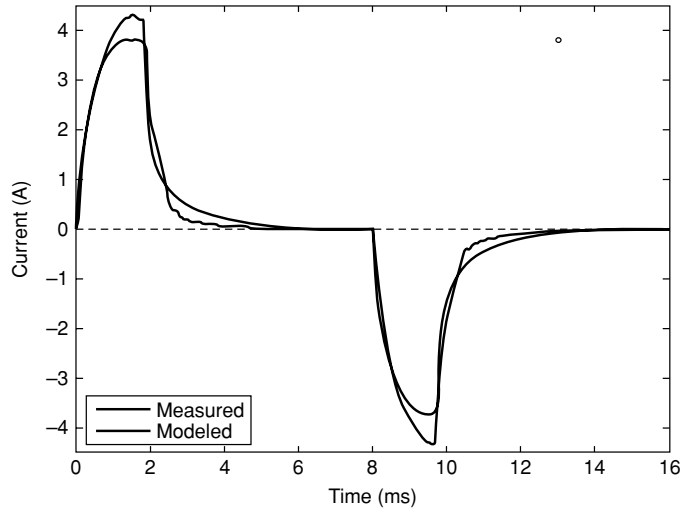

FIGURE 16.36 Comparison of computer-modeled and measured currents in the hammer valve of Figures 16.34 and 16.35 operating a typical hydraulic circuit, driven by 24 V switched at 62.5 Hz. The measured curve has slightly greater peak amplitude than the modeled curve. Reprinted by permission from *Int J Fluid Power* [20].

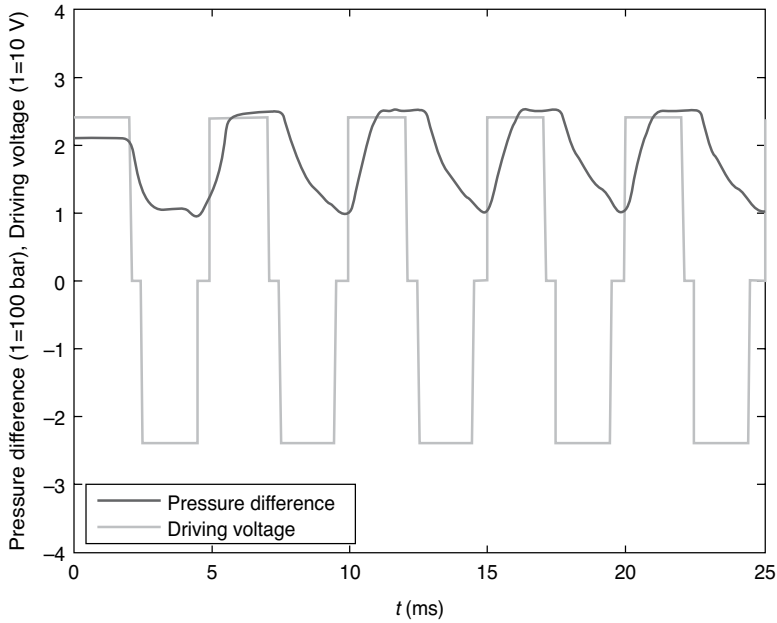

FIGURE 16.37 Measured pressure difference and driving voltage waveforms at 200 Hz switching rate in hammer valve of Figure 16.35. Reprinted by permission from *Int J Fluid Power* [20].

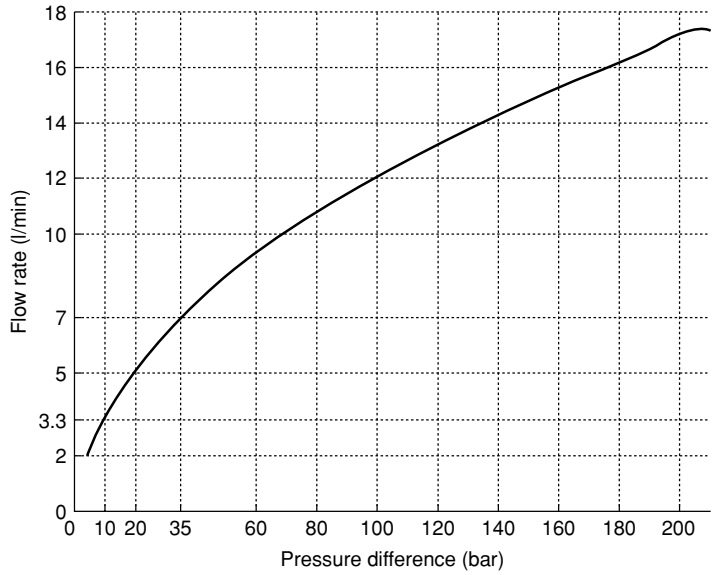

FIGURE 16.38 Measured pressure difference versus flow rate (in liters per minute) for hammer valve of Figure 16.35 with 210 bar input supply pressure and hydraulic oil temperature of 30°C. Reprinted by permission from *Int J Fluid Power* [20].

It remains to be seen whether digital hydraulics will become as commonplace as digital electronics. A recent application of digital hydraulics is flow control in petroleum production, particularly for waterflood injector wells [22].

PROBLEMS

16.1 Use SPICE to solve Example 16.1 with $R_1 = 2$ MPa s/m^3 and $R_2 = 4$ MPa s/m^3. Compare your results with simple electric circuit theory.

16.2 Use SPICE to solve Example 16.1 with $R_1 = 3$ MPa s/m^3 and $R_2 = 5$ MPa s/m^3. Compare your results with simple electric circuit theory.

16.3 Redo Example 16.2 using both SPICE and the quadratic formula for $K = 1$, $R = 1$, and source pressure $P_S = 10$ Pa.

16.4 Redo Example 16.2 using both SPICE and the quadratic formula for $K = 2$, $R = 1$, and source pressure $P_S = 10$ Pa.

16.5 Redo Example 16.2 using both SPICE and the quadratic formula for $K = 1$, $R = 2$, and source pressure $P_S = 10$ Pa.

16.6 Redo Example 16.2 using both SPICE and the quadratic formula for $K = 2$, $R = 2$, and source pressure $P_S = 10$ Pa.

16.7 Use SPICE to solve Example 16.3 with $Q = 10$ m^3/s, $R = 50$ Pa s/m^3, and $C = 100$E–6 m^3/Pa. Find the time constant of your results and compare it with RC.

16.8 Use SPICE to solve Example 16.3 with $Q = 10$ m^3/s, $R = 50$ Pa s/m^3, and $C = 50$E–6 m^3/Pa. Find the time constant of your results and compare it with RC.

REFERENCES

1. Brauer JR, Lumkes Jr. JH. Coupled model of a magnetically-actuated valve controlling a hydraulic cylinder and load. *IEEE Trans Magn* 2002;38:917–920.
2. Brauer JR. Electromagnetic analogies for modeling hydraulics. *Int Compumag Soc Newsl* 2000;7:3–5.
3. White FM. *Fluid Mechanics*, 2nd ed. New York: McGraw-Hill Book Co.; 1986.
4. Slater JG, Wanke T, Bitant J. *Introduction to Hydraulics Seminar Manual*. Milwaukee, WI: Milwaukee School of Engineering Fluid Power Institute; 2005.
5. Giles RV, Evett JB, Liu C. *Fluid Mechanics and Hydraulics*, 3rd ed. New York: McGraw-Hill Book Co.; 1994.
6. Brauer JR (ed.). *What Every Engineer Should Know About Finite Element Analysis*, 2nd ed. New York: Marcel Dekker, Inc.; 1993.
7. Rausch M, Gebhardt M, Kaltenbacher M, Landes H. Computer-aided design of clinical magnetic resonance imaging scanners by coupled magnetomechanical-acoustic modeling. *IEEE Trans Magn* 2005;41:72–81.

8. Tallbaeck GR, Lavers JD, Erraki A, Beitelman LS. Influence of model parameters on 3-D turbulent flow in an electromagnetic stirring system for continuous billet casting. *IEEE Trans Magn* 2004;40:597–600.
9. Brauer JR, Lumkes JH Jr., Slater JG. Coupled electromagnetic and hydraulic devices modeled by finite elements and circuits, *Digests of IEEE Conference on Electromagnetic Field Computation*, Milwaukee, WI, June 2000.
10. Brauer JR, Lumkes Jr. JH. Electrohydraulic systems simulations containing electromagnetic finite element models of magnetic actuators, *SAE Off-Highway & Powerplant Congress*, Milwaukee, WI, Sept. 2000, paper 2000-01-2633.
11. Johnson JL. *Design of Electrohydraulic Systems for Industrial Motion Control*. Cleveland, OH: Parker Corp.; 1991.
12. Brauer JR. Model of a Chopper-driven magnetic actuator in an electrohydraulic system, *Proceedings of the IEEE International Electric Machines and Drives Conference,* Cambridge, MA, June 2001.
13. Lumkes Jr. JH. *Control Strategies for Dynamic Systems*. New York: Marcel Dekker, Inc.; 2002.
14. Merritt HE. *Hydraulic Control Systems*. New York: John Wiley & Sons, 1967.
15. Brauer JR, Lumkes Jr. JH, Lin D. Modeling an electronically-controlled magnetic actuator operating a hydraulic valve and cylinder, *Proceedings of the International Fluid Power Expo/SAE/National Fluid Power Conference*, Las Vegas, NV, March 2002.
16. Brauer JR. Magnetic actuator models including prediction of nonlinear eddy current effects and coupling to hydraulics and mechanics, *Proceedings of Congresso Brasileiro de Eletromagnetismo*, Gramado, Brazil, November 2002.
17. Brauer JR, Mayergoyz ID. Finite element computation of nonlinear magnetic diffusion and its effects when coupled to electrical, mechanical, and hydraulic systems. *IEEE Trans Magn* 2004;40:537–540.
18. Solveson M, Christini M, Collins D. Actuator design: meeting your customer's requirements for success, Presentation at *ANSYS First-Pass System Success Workshop*, Southfield, MI, October 2008.
19. Uusitalo JP, A novel digital hydraulic valve package: a fast and small multiphysics design, Ph.D. thesis, Tampere University, Finland (2010).
20. Uusitalo JP, Ahola V, Söderlund L, Linjama M, Juhola M, Kettunen L. Novel bistable hammer valve for digital hydraulics. *Int J Fluid Power* 2010;11:35–44.
21. Uusitalo JP, Söderlund L, Kettunen L, Linjama M, Vilenius M. Dynamic analysis of a bistable actuator for digital hydraulics. *IET Science, Meas & Techn* 2009;3:235–243.
22. Konopscynski M. *A Sign of Good Things to Come?*, Oilfield Technology, May 2012.